Solar Energy Materials & Solar Cells 207 (2020) 110353

Contents lists available at ScienceDirect

Solar Energy Materials and Solar Cells

journal homepage: http://www.elsevier.com/locate/solmat

Hydrogen-induced degradation: Explaining the mechanism behind light- and elevated temperature-induced degradation in *n*- and *p-type* silicon

Daniel Chen *, Phillip Hamer, Moonyong Kim, Catherine Chan, Alison Ciesla nee Wenham, Fiacre Rougieux, Yuchao Zhang, Malcolm Abbott, Brett Hallam

School of Photovoltaic and Renewable Energy Engineering, The University of New South Wales, Kensington, NSW, 2052, Australia

ARTICLE INFO

Keywords:
LeTID
Surface-related degradation
n-type silicon
p-type silicon
Hydrogen
Emitter diffusion
Hydrogen-induced degradation

ABSTRACT

Light- and elevated temperature-induced degradation (LeTID) has been extensively studied on *p-type* silicon materials with increasing evidence suggesting the involvement of hydrogen. Recent findings of the identical phenomenon in *n-type* silicon wafers have further opened up new areas of understanding into the inherent behavior and root cause of the defect. In this work, we compare LeTID observed in both *p-* and *n-type* silicon wafers under both dark and illuminated annealing conditions, highlighting previously unobserved similarities in defect formation and recovery kinetics. We report thermal activation energies of the LeTID-related degradation and recovery in *n-type* silicon to be 0.76 ± 0.02 eV and 0.97 ± 0.01 eV without illumination, respectively, and 0.70 ± 0.05 eV and 0.83 ± 0.15 eV under illumination (0.02 kWm^{-2}), respectively. Furthermore, we present additional experimentation demonstrating the thermal and illumination dependency of surface-related degradation (SRD) in *n-type* silicon. We report an extracted activation energy of this SRD of 0.38 ± 0.10 eV. Through modelling of the hydrogen charge state fractions, we speculate that the behavior of LeTID both in the dark and under illumination may be explained by the migration of and interactions between charged hydrogen species and dopant atoms within the diffused layers and the silicon bulk.

1. Introduction

Since its discovery by Ramspeck et al. in 2012 [1], light- and elevated temperature-induced degradation (LeTID) [2] has received noteworthy attention in both academia and the global photovoltaics industry. Initially observed in boron-doped *p-type* multicrystalline silicon (*mc-Si*) passivated emitter and rear cell (PERC) devices, this phenomena was found to result in up to a $16\%_{rel}$ drop in efficiency [3]. Similar analysis on various materials such as gallium-doped wafers additionally ruled out the possibility of the more commonly known boron-oxygen (BO) related light-induced degradation (LID) and iron-boron dissociation mechanisms [1]. Since then, numerous studies have been conducted to understand the kinetics of defect formation and regeneration [2,4–11]. Various studies observed a modulation of the LeTID severity with the peak fast-firing temperature [12–15]. Another key finding from UNSW by Chan et al. was the appearance of LeTID at elevated temperatures in the absence of illumination which was speculated to be caused by thermally-induced excess carriers [5]. The understanding that LeTID could form in the dark led to an alternative testing strategy for various other materials, primarily *p-type* Czochralski-grown silicon (*Cz-Si*), which typically submits to BO-related LID under illumination [16,17]. A study by Fertig et al. and our previous work later identified that LeTID not only exists in *mc-Si* materials but also in *p-type Cz-Si* as well [18,19]. This finding strengthened the notion that LeTID was a universal defect occurring in all silicon materials, with findings of degradation on float-zoned (FZ) silicon later proposed to have an identical root cause [20,21].

The intense research effort aimed at identifying the nature of LeTID has generated a range of hypothesis for its constituents, the most common of which are metallic impurities [14,22–26]. However, there is now surmounting evidence highlighting the involvement of hydrogen [5,27–35]. Some of these studies have placed emphasis on the properties of the passivating dielectric layers in particular the hydrogenated silicon nitride (SiN_x:H) film, which is known to release hydrogen into the silicon bulk during firing [31,33,34,36]. Jensen et al. further demonstrated LeTID through plasma hydrogenation, thus relating the phenomena to the hydrogen source itself and not the fast-firing process [32].

More recent work involving hydrogenated *n-type* silicon showed that

* Corresponding author.
E-mail address: daniel.chen@unsw.edu.au (D. Chen).

https://doi.org/10.1016/j.solmat.2019.110353
Received 20 July 2019; Received in revised form 7 December 2019; Accepted 9 December 2019
Available online 26 December 2019

such material was also susceptible to LeTID [37–39]. Our earlier work in Ref. [39] noted similar findings to Renevier *et al.* whom, many years earlier, observed an unknown form of bulk degradation in *n-type* silicon [40]. Prior work on undiffused *n-type* FZ wafers did not observe any degradation, thus LeTID degradation in *n-type* silicon was thought to either not activate, form on a different time scale or in different quantities [41]. In our work, we instead observed that the defect concentration and formation kinetics relied heavily on the presence of and polarity of the surface emitter layers. With a boron-diffusion, the bulk degradation due to LeTID is distinct and was found to form in identical time scales *p-type* wafers [39]. With a phosphorus diffusion, the kinetics were found to be accelerated by several orders of magnitude. We concluded that the emitters played a role in facilitating hydrogen in-diffusion and trapping during firing. We also identified a way of rapidly inducing surface-related degradation (SRD), a phenomena which appears to occur usually during or after LeTID recovery or after LeTID mitigation treatments [42]. Although the kinetics and properties of such degradation on *p-type* silicon materials has been meticulously studied by Sperber et al. [42–44], the accelerated appearance of SRD in n-type Si, particularly at reduced temperatures and illumination intensities, has not been previously studied.

In this study, we extend our work in Ref. [39] and present new findings regarding the behaviours of LeTID in *n-type* silicon. Firstly, by using *p-* and *n-type* silicon wafers processed in parallel, we examine similar degradation time scales in both the dark and under illumination for the two vastly different materials. We further explore the degradation and regeneration behaviour of phosphorus-diffused *n-type* silicon as an extension of our work in Ref. [39], demonstrating that instead of a further acceleration in these reaction kinetics under illumination as would be expected for a carrier-induced process, we instead observe a reduction. Secondly, we investigate the rapid onset of SRD in phosphorus diffused *n-type* silicon at reduced carrier injection and investigate its dependence on both illumination and temperature. We use a Sah-Shockley based hydrogen charge state occupancy model [45] to describe the motion of atomic hydrogen in the vicinity of a p-n junction or a high-low junction, testing the hypothesis that the interactions between charged hydrogen atoms and dopant atoms in the diffused layers dictate the rate at which hydrogen will diffuse towards the surface. Lastly, we propose a model of the electric fields generated by a diffused region to give a possible explanation regarding the formation of precursors for hydrogen-induced SRD.

2. Methodology

2.1. Sample preparation

To investigate the influence of emitter polarity on the defect formation and regeneration kinetics of LeTID, we fabricated lifetime test structures using commercially bought (*Woongjin Solar*), 6-inch uncompensated *n-type Cz-Si* wafers with a resistivity of 2 Ω cm. As a comparison to conventional structures commonly presented in various literature, *p-type* commercial multicrystalline silicon (*mc-Si*) wafers from adjacent 'sistering' positions in an ingot with a resistivity of 1.6 Ω cm and thickness of 190 ± 6 μm from *GCL Poly* were processed as well. For reference, these *mc-Si* wafers are from the same ingot as wafers used in Refs. [19,39]. As-cut *Cz-Si* wafers were placed in KOH solution to remove saw damage and subsequently textured to a final thickness of 180 ± 3 μm in an alkaline texturing bath. *Mc-Si* wafers were iso-textured via an external party, with a final thickness of 177 ± 5 μm. We acknowledge that Bredemeier et al. identified differences in measured LeTID defect concentration with varying wafer thickness [46], however, it is assumed that the small discrepancy in thickness present in the two materials would not have a noticeable impact. Once textured, all wafers were then split into various diffusion groups as depicted in Fig. 1 below. Both *p-type* and *n-type* wafers were first cleaned using a cleaning sequence proposed by the Radio Corporation of America (RCA) in preparation for diffusion. This cleaning consists of; a 6 min dip in ammonium hydroxide (NH_3OH) and hydrogen peroxide (H_2O_2) solution (RCA1), a rinse in deionized (DI) water and a subsequent 6 min clean in a solution of hydrochloric acid (HCl) and hydrogen peroxide (RCA2) followed by another rinse in DI water. This is then followed by a short dip in 2 vol% dilute hydrofluoric acid (DHF) to remove any oxides that may be present on the surface.

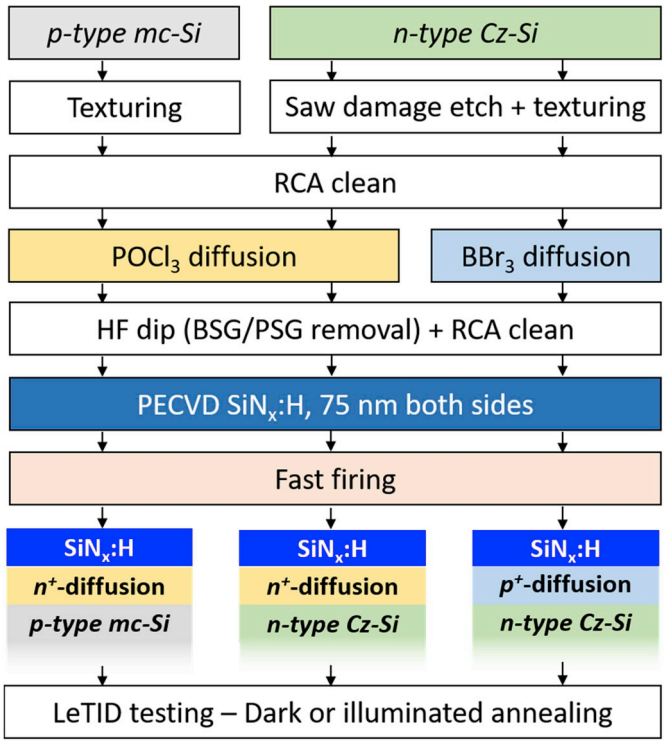

Fig. 1. Process flow chart for processing of symmetrical *n-* and *p-type* lifetime test structures with varying emitter polarity for LeTID testing.

N-type *Cz-Si* underwent a boron diffusion in a quartz tube using a boron tribromide (BBr_3) source at the peak temperature of approximately 920 °C resulting in a p^+-emitter with a sheet resistance of R_{sheet} = (110 ± 3) Ω/□ on both sides. The reported sheet resistance is measured from a 120 mm × 120 mm region in the center of the wafer where the diffusion uniformity is higher and where samples used for this experiment are cut from. Under these conditions, we can avoid the generation of any defect associated with misfit dislocations and lattice damage usually associated with boron diffusions as reported by Cousins and Cotter [47]. Additionally, another group of both *n-type* and *p-type* wafers underwent a phosphorus diffusion in a quartz tube using a phosphoryl chloride ($POCl_3$) source resulting in dual-sided n^+-emitters of R_{sheet} = (65 ± 7) Ω/□. All diffused samples were then given a short treatment in DHF to remove any borosilicate glass (BSG) or phosphosilicate glass (PSG) left on the surface after diffusion. Electrically active dopant profiles (see Fig. 2) for further simulations were subsequently measured on dummy wafers diffused in parallel using an electrochemical capacitance voltage (ECV) tool. Non-diffused structures were not fabricated in this work as our previous studies indicated that fast-firing of n-type wafers in the absence of an emitter did not instigate LeTID formation, but instead showed SRD [39].

All wafers were then RCA cleaned again prior to the deposition of dielectric films. A 75 nm layer of hydrogenated silicon nitride film (SiN_x:H) with a refractive index of 2.08 at 633 nm [48] was deposited using a remote plasma enhanced chemical vapor deposition tool (Meyer Burger, MAiA) [49]. To introduce hydrogen into the silicon bulk from the SiN_x:H films, wafers were fired at a peak temperature of 744 °C using a Schmid infrared inline metallization belt furnace at a speed of 4.5 m/min. Actual

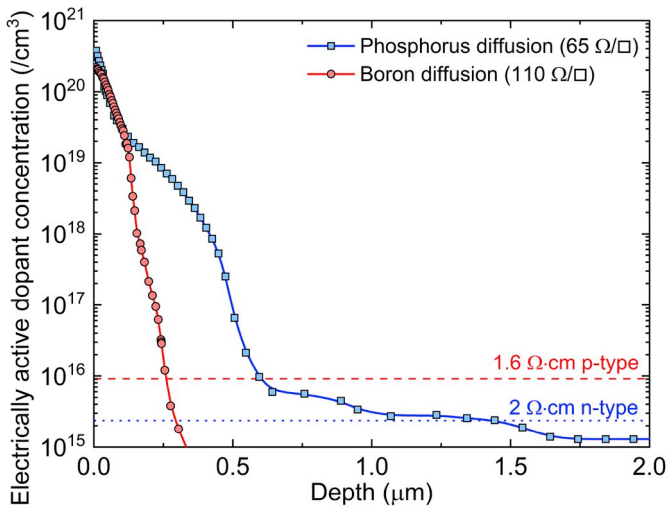

Fig. 2. Electrically actively depth-resolved dopant profiles of phosphorus (square) and boron (circle) diffusions measured using ECV. Dashed and dotted lines mark the background dopant concentrations for 1.6 Ω cm *p-type* and 2 Ω cm *n-type* wafers, respectively. Solid lines are provided as a guide to the eyes.

temperatures were measured on identical dummy wafers using a Q13 Datapaq temperature profiler averaged using three K-type thermocouples (Omega KMQXL-IM075G-300). The thermal profile for this firing process can be found in Ref. [39]. Samples were then laser cleaved into 52 mm × 52 mm tokens prior to LeTID testing. Due to edge non-uniformities as the result of wafer contact with the diffusion boat, the central token from each substrate was taken for experimental use.

2.2. Testing for LeTID

LeTID testing in this study was conducted *in-situ* at elevated temperature on a quasi-steady-state photoconductance (QSSPC) tool with a temperature controlled stage (Sinton Instruments, WCT-120TS) [50]. For instances of illuminated annealing, a variable-intensity halogen incandescent lamp is combined with the QSSPC setup to allow for illumination directly on the measurements stage. The lamp is turned off for a period of 3 s whilst the QSSPC measurements is taken. The lamp intensity is measured using a PM100D power meter and a S350C sensor (Thorlabs) and is reported in kWm^{-2} unless specified otherwise. Due to the spectral mismatch between the halogen lamp and the 1-sun "AM1.5G″ spectrum, the "suns equivalent" illumination is approximated by comparing the short-circuit current (I_{SC}) of a BO stabilised PERC reference solar cell under the treatment illumination to that under a solar simulator (i.e. for reference, a measured power density of 1 kWm^{-2} under the halogen lamp corresponds to approximately 0.91 suns equivalent). For further deliberation of the unit of "suns equivalent", the reader is referred to Ref. [51]. Measurements of minority carrier lifetime were analysed using the generalised method [52] and intrinsic recombination was corrected using the parametrization by Richter et al. [53]. Due to the temperature dependence of carrier mobility, a correction based upon the Dorkel-Leturcq mobility model [54] was applied to measurements taken at elevated temperatures (>30 °C). Effective minority carrier lifetimes (τ_{eff}) were extracted at an injection level (Δn) equal to approximately 10% of the background dopant density N_{dop} (i.e. $\Delta n = 2.4 \times 10^{14}$ cm^{-3} for *n-type* and $\Delta n = 9.1 \times 10^{14}$ cm^{-3} for *p-type* samples). In this paper the evolution in carrier lifetime due to LeTID is presented using normalised τ_{eff} and the apparent defect concentration (N^*_{app}). This N^*_{app} metric can be described by the equation [55]:

$$N^*_{app}(t) = \frac{1}{\tau(t)} - \frac{1}{\tau(t=0)} \quad (1)$$

Where τ(t) denotes the effective minority carrier lifetime measured during LeTID testing and τ(t = 0) is the lifetime measured directly after firing and before any additional thermal processes. Note that this approach assumes that the amount of LeTID that may pre-form during the firing process [19] is negligible compared to the quantity formed during testing. In this work, N^*_{app} is used to provide a qualitative assessment of the defect behaviour rather than an absolute exact quantification of the LeTID defect density. This is because both SRD and bulk degradation are observed to occur in parallel, thus misrepresenting the exact bulk defect concentration. Likewise, the apparent dark saturation current density (J_{0s}) extracted using the method proposed by Kimmerle et al. is used to give a qualitative assessment of the surface conditions [56].

3. Results

3.1. The influence of emitter polarity on LeTID in n- and p-type silicon

Although the dark annealing and illuminated annealing of *p-type* and *n-type* silicon have been demonstrated separately in prior literature, no other work to our knowledge has shown comparisons in defect kinetics together. A comparison of the evolutions in τ_{eff} on both *p-type* and *n-type* samples is depicted in Fig. 3(a). In the dark, both boron-diffused n-type samples (blue downward triangles) and phosphorus-diffused *p-type* samples (red squares) exhibit bulk degradation on similar time scales (≈25 h). The small dip in lifetime appearing on the boron-diffused n-type samples at approximately 1000 s may be due to partial LeTID formation as a consequence of illumination from the QSSPC flash and the measurement frequency. With the addition of illumination (≈1 kWm^{-2}), the time required for the boron-diffused *n-type* samples (blue circles) and phosphorus-diffused *p-type* samples (orange squares) to reach a point of maximum degradation is accelerated by 1.5 orders of magnitude, again with surprisingly similar time scales.

In the case of phosphorus-diffused *n-type* samples (green leftward triangles), the time scales during dark annealing agree with our prior findings in Ref. [39], i.e. the degradation and regeneration kinetics are over 1.5 orders of magnitude faster than the boron-diffused counterparts. We note that the τ_{eff} of all samples prior to degradation was measured to be in a close range of 340 ± 40 μs, thus the differences in the excess carrier concentration (Δn) alone cannot be substantial enough to entirely explain the dissimilar kinetics. Interestingly, when this structure is annealed under illumination (green upward triangles), instead of a further acceleration of degradation and regeneration as would typically be expected for a carrier-induced defect, we observe a reduction in the overall reaction kinetics. Surprisingly, all three structures under illumination appear to reach the maximum degradation at similar time scales. At first glance, under illumination, the recovery in τ_{eff} of all three structures appears to be affected by a counteracting degradation reaction. In Fig. 3(c), the extracted J_{0s} indicate an increase in the surface recombination with prolonged annealing, suggesting the involvement of SRD.

In addition, analysis of the N^*_{app} (see Fig. 3(b)) shows a significantly lower maximum defect concentration in the *n-type* wafers (8.2×10^{-4} μs^{-1}) when compared to the *p-type* wafers (5.7×10^{-3} μs^{-1}), which will be discussed in Section 4.1.

3.2. The impact of illumination and temperature on phosphorus-diffused n-type silicon

In the previous section, we highlighted the unexpected behavior in phosphorus-diffused *n-type* silicon wafers where added illumination reduced the apparent degradation or recovery reaction rates. A further experiment was undertaken to observe the dependence of both the degradation rate as well as surface degradation in response to changes in temperature and illumination. Phosphorus diffused *n-type Cz-Si* samples

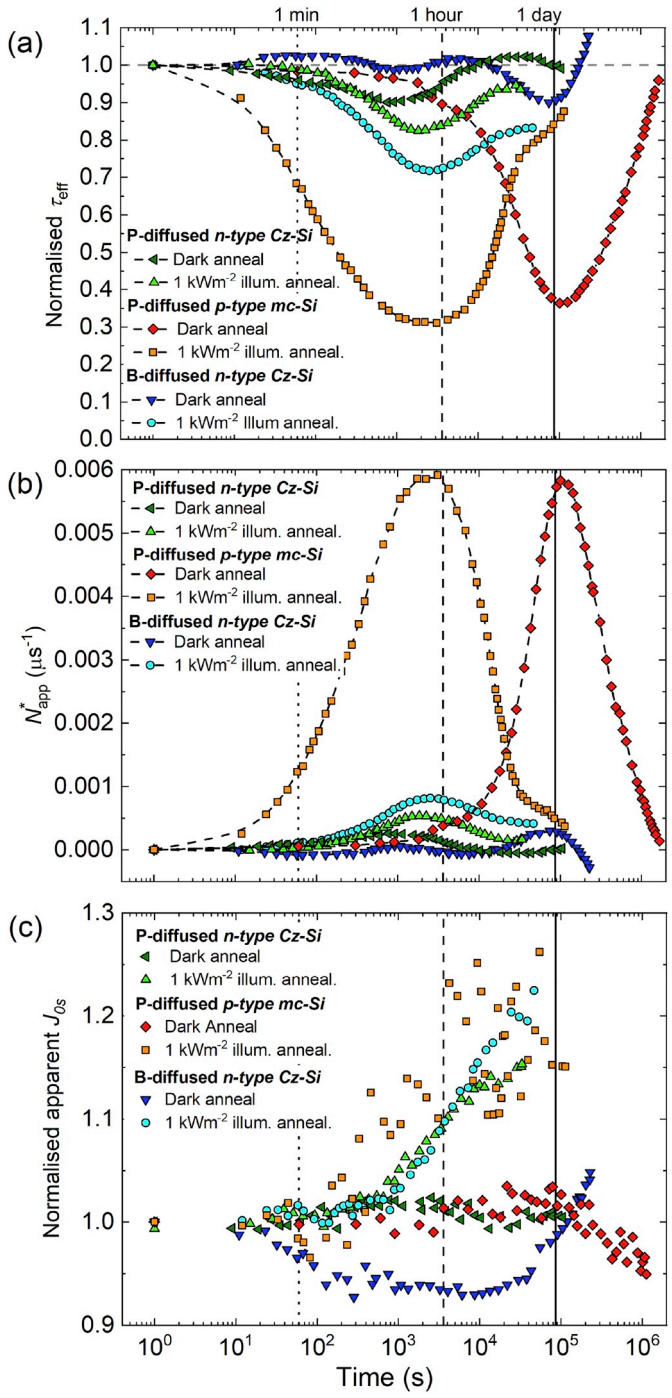

Fig. 3. Comparison of LeTID degradation and recovery in boron and phosphorus diffused *n-type Cz-Si* and phosphorus diffused *p-type mc-Si* silicon showing: (a) τ_{eff} normalised to the lifetime after firing, (b) apparent defect concentration (N^*_{app}) and (c) normalised apparent J_{0s}. Measurements were taken *in-situ* at a temperature of approximately 160 ± 4 °C. Dashed lines are provided as a guide for the eyes. (For interpretation of the references to color in this figure legend, the reader is referred to the Web version of this article.)

taken from the identical group to those described in the previous section were characterized *in-situ* at a range of temperatures between 140 ± 4 °C and 175 ± 4 °C. Samples were either dark annealed or exposed to an illumination intensity of approximately 0.02 kWm^{-2} supplied by a single variable intensity broadband halogen lamp. τ_{eff} and N^*_{app} as a function of annealing duration is shown in Fig. 4(a) and b, respectively.

In the dark, the temperature-dependence of the defect formation follows a similar trend to that found in *n-type* silicon wafers in Refs. [38, 39] (Fig. 4(a)). Increasing the substrate temperature accelerates both degradation and regeneration reactions and reduces the maximum perceived degradation extent. With added low-intensity (0.02 kWm^{-2}) illumination, however, instead of displaying any signs of recovery from LeTID, an inflection point followed by a secondary degradation attributed to surface degradation appears. The time scale for reaching the point of inflection, however, appears to be slower under illumination for identical temperatures than in the dark, thus consistent with the results in Section 3.1. Given that any further degradation, for example, at the surface should help to accentuate the degradation rate if compounded with LeTID defect formation, this result suggests a significant reduction of the LeTID-related degradation and regeneration rates.

The degradation and recovery rates were obtained by assuming that all reactions occur simultaneously, using the following equation:

$$N^*_{app}(t) = N^*_{app,bulk}\left\{\left[f_{fast}\left(1-\exp\left(-k_{fast}t\right)\right)\right] + \left[f_{slow}\left(1-\exp\left(-k_{slow}t\right)\right)\right] + \left[\exp\left(-k_{rec}t\right)-1\right]\right\} + N^*_{app,SRD}\left(1-\exp\left(-k_{SRD}t\right)\right) \quad (2)$$

where $N^*_{app,bulk}$ is the maximum N^*_{app} attributed by the bulk degradation,

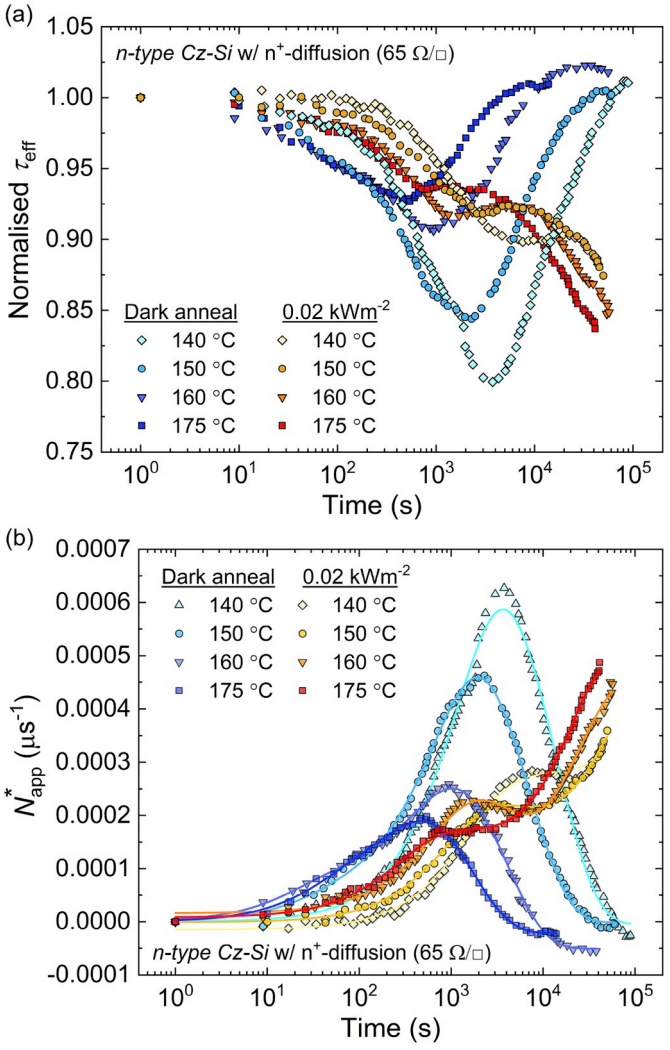

Fig. 4. (a) Normalised τ_{eff} (extracted at $\Delta n = 2.4 \times 10^{14}$ cm^{-3}) as a function of time for *n-type*, phosphorus-diffused samples dark annealed (blue colors) or illuminated annealed (0.02 kWm^{-2}) (red colors) at a temperature range between 140 °C and 175 °C. (b) The corresponding apparent defect concentration. The solid lines are fit using Eq. (2) (For interpretation of the references to color in this figure legend, the reader is referred to the Web version of this article.)

f_{fast} and f_{slow} are the proportion of defects pertaining to two observed degradation reactions (a fast-forming and a slow forming) (where $f_{fast} + f_{slow} \leq 1$ and $f_{fast} \geq f_{slow}$), k_{fast} and k_{fast} are the respective degradation rates, k_{rec} is the rate of recovery, $N^*_{app,SRD}$ is the maximum N^*_{app} contributed to by SRD, and k_{SRD} is the rate of SRD. This fitted model assumes that the extracted rates are constant across the experiment and thus, are not affected by the observed changes in lifetime. Using Eq. (2), the experiment results were fitted as shown in Fig. 4(a). For the results without illumination, $N^*_{app,SRD}$ was equal to 0 as no SRD was observed. Under illumination, the fast-forming degradation either did not occur or was not significant such that $f_{fast} = 0$.

Fig. 5 shows the Arrhenius plot of the degradation and recovery rate constants for both dark annealed and illuminated annealed samples according to Eq. (2). Based on the fits in Fig. 4(b), the activation energies for degradation ($E_{A,deg,DA/LS,fast/slow}$), recovery ($E_{A,rec,DA/LS}$) and for SRD under illumination ($E_{A,SRD}$) were extracted using the Arrhenius function defined by:

$$k(T) = k_0 \exp\left(-\frac{E_A}{k_B T}\right) \quad (3)$$

where k_0 is the characteristic attempt frequency, k_B is the Boltzmann constant and E_A is the associated activation energy. For the primary bulk degradation components in the dark and under illumination ($Deg_{DA,\ slow}$ and $Deg_{LS,\ slow}$), we determine similar activation energies of $E_{A,deg,DA,\ slow} = 0.76 \pm 0.02$ eV and $E_{A,deg,LS,slow} = 0.70 \pm 0.05$ eV, respectively. The recovery rate of the LeTID component also demonstrated similarities under both conditions of dark annealing and illuminated annealing with $E_{A,rec,DA} = 0.97 \pm 0.01$ eV and $E_{A,rec,LS} = 0.83 \pm 0.15$ eV, respectively. We note that both the degradation and recovery activation energies are lower than what has been reported in the literature for LeTID (Vargas et al. reported an activation energy of 1.08 ± 0.05 eV for degradation and 1.11 ± 0.04 eV for recovery in the dark on *p-type mc-Si* [57]). It is possible that these differences may be due to the different materials used (e.g. *mc-Si* vs. *Cz-Si*), particularly if hydrogen is involved in LeTID degradation and recovery. This is because the movement of hydrogen is complicated and hindered by its interactions with defect states throughout the silicon bulk.

Furthermore, we determine the thermal activation energy of two additional components: 1) A fast bulk degradation reaction observed only during dark annealing ($Deg_{DA,\ fast}$) with $E_{A,deg,DA,fast} = 0.3 \pm 0.1$ eV. This reaction appears to have little to no temperature dependency and was not observed during light soaking. 2) The SRD observed under illumination is determined to have an $E_{A,SRD} = 0.38 \pm 0.1$ eV. The large error in this value may be due to the accuracy in fitting whilst decoupling the SRD component from the LeTID recovery component. Despite this, the extracted value appears to be much lower than the value extracted by Sperber et al. (1.06 ± 0.03 eV) on *p-type mc-Si* [21]. Although our result also suggests that surface degradation is thermally activated, in line with the assessment by Sperber et al. [21], the exact meaning of this activation energy remains unclear and requires further investigation. A more theoretical approach to understanding the physical mechanism behind SRD is discussed in Section 4.4.

An investigation into whether the SRD component also responds to changes in illumination is also carried out. Samples from identical sister groups were annealed at a fixed temperature of 160 °C but using a variable illumination intensity with power density between 0.02 kWm^{-2} and 1.5 kWm^{-2}. The changes in both effective lifetime (Fig. 6(a)) and surface quality (Fig. 6(b)) show a distinct correlation between the transition from bulk LeTID degradation to SRD and the supplied illumination intensity. At lower intensities, we observe identical behaviors to those seen in Fig. 4 where a secondary SRD dominates the τ_{eff} at longer time scales. As the illumination intensity is increased, the degree

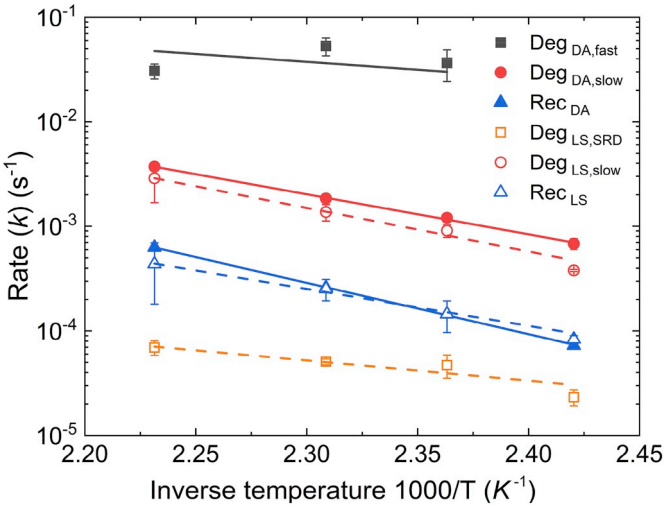

Fig. 5. Degradation (Deg) and recovery (Rec) rates for dark annealing (closed symbols, solid lines) and illuminated annealing (0.02 kWm^{-2}) (open symbols, dashed lines) as a function of temperature of *n-type* phosphorus-diffused samples. Lines correspond to a fit for Arrhenius analysis.

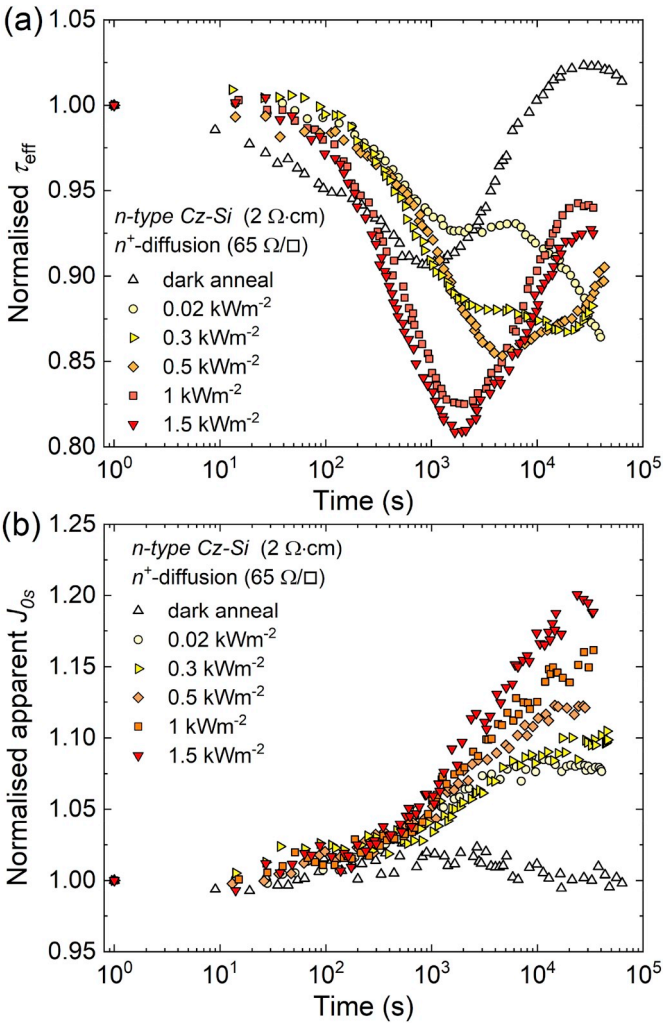

Fig. 6. (a) Normalised τ_{eff} and (b) normalised apparent J_{0s} as a function of time for *n-type*, phosphorus diffused annealed at 160 °C under a varying illumination intensity between 0.02 kWm^{-2} and 1.5 kWm^{-2}. Control samples are annealed in the dark at identical temperatures (white triangle). (For interpretation of the references to color in this figure legend, the reader is referred to the Web version of this article.)

to which a secondary degradation is observed begins to decrease. Instead, both bulk LeTID degradation and recovery rates increased in conjunction with the extent of SRD. One possible explanation for this observation is that either the illumination dependence of the recovery rate is greater than that of the degradation rate, such that the maximum bulk degradation is reduced. The other possible explanation is that the LeTID-related degradation and SRD are interdependent under illumination such that an increase in the SRD extent reduces the LeTID extent and vice versa. As both degradation mechanisms are likely related, this interdependency is quite likely, although further work is required to isolate the effects.

4. Discussion

4.1. LeTID in n- and p-type silicon

This area of discussion pertains to the observations in Section 3.1. The first peculiar observation is the matching degradation time scales of the three different materials under illumination. Given the significant disparity in materials used and diffusion profiles on each sample, this suggests that the degradation behaviour may be governed by processes identical to all samples such as PECVD SiN_x:H deposition, firing conditions and in relation, the relative hydrogen distributions throughout the wafers. Although we cannot exclude the possibility that matching time scales for degradation under illumination in all specimens may be simply a coincidence, we are confident with regards to the change in behavioural kinetics between dark annealed and illuminated annealed samples. The differences in the maximum extracted N^*_{app} between *p-type mc-Si* and *n-type Cz-Si* may be explained using two equally likely occurrences. The first is that the absolute hydrogen concentration diffusing into the wafer and contributing to LeTID is much greater in *p-type mc-Si* than in *n-type Cz-Si*. This may be expected in *mc-Si* given not only the enhanced hydrogen diffusivity down grain boundaries [58], but the larger concentrations of defects and impurity trap sites for hydrogen to form bound states with within the bulk. A reduced solubility of hydrogen in *n-type* silicon also results in a larger concentration of hydrogen being localized close to the surface of the wafer [39,59,60]. The second possible explanation is that hydrogen may not be the single limiting factor for LeTID formation and a secondary candidate inherent to the wafer source is required. Another notable observation, the evolution in J_{0s} (Fig. 3(c)) suggests that all samples undergoing the illuminated degradation treatment experience an additional decline in the apparent surface quality. This degradation has been extensively studied in the context of LeTID and some works have suggested the involvement of hydrogen build-up near the surface [39,42,61,62]. Our work in Ref. [39] speculated that hydrogen may diffuse towards the surface of the silicon wafer during prolonged annealing treatments, resulting in the formation of hydrogen-induced extended defects. Possible mechanisms to explain these surface phenomenon will be conjectured in Section 4.4.

It is also important to point out that the behaviours we observe in this work and in Ref. [30] are partially in contradiction with the observations made by Sio et al. in Ref. [37]. It was observed in Ref. [37] that the degradation in *n-type cast-mono* silicon occurred on a much slower time scale than that in *p-type* materials. However, the authors pointed out that wafers were annealed at 200 °C for 15 min, which, is known to change the kinetics of LeTID [5,63]. If this is the case, the influence of pre-annealing treatments on *n-type* silicon should be explored in future work.

Overall, in the experiments presented in Section 3.1 and 3.2, there are several intriguing observations drawn from the experimental results regarding defect kinetics that we will aim to address within the following sections:

1) Reaction kinetics on samples with a p-n junction, for example, a phosphorus diffused *p-type* silicon wafer or a boron-diffused *n-type* silicon wafer appears to be significantly slower than on samples with a high-low junction (e.g. phosphorus diffused *n-type* silicon).
2) The degradation time scale appears to slow down in phosphorus diffused *n-type* silicon upon exposure to illumination, contrary to what is expected for carrier induced degradation. However, identical time scales for degradation are observed for all materials under sufficient illumination.
3) The onset of SRD occurs rapidly under illumination on *n-type* silicon samples with a high-low junction.

4.2. Modelling hydrogen charge states: interactions with doped layers

Although the recombination active species responsible for LeTID is not yet known, there is a substantial amount of evidence highlighting the involvement of hydrogen as a primary factor. Both experimental and theoretical work have suggested that the recovery mechanism of LeTID may be related to either the diffusion of hydrogen into the wafer to passivate the recombination active species [46] or effusion out of the silicon wafer where it no longer contributes to the recombination activity [39,64]. If we were to accept the latter explanation for LeTID recovery, then the concentration of hydrogen, its charge state and its location in the silicon wafer will all play a crucial role in degradation and recovery kinetics. The motion of hydrogen in this case could be limited by its interaction with various charged impurities and particles, in particular, dopant atoms in heavily doped regions [64].

To address the three points above, we simulate the interactions between various charged species of hydrogen in close proximity to a doped layer on both *n-type* and *p-type* silicon materials. We use a Sah-Shockley model derived from the work from Sun et al. [45] that is an extension to the models developed by Herring et al. [65] and Hallam et al. [66] to estimate the occupancy fraction of the various hydrogen charge states. Using the measured active dopant profiles from ECV measurements (see Fig. 2), we are able to obtain the probability of occupancy of hydrogen for all three charge states as a function of depth into our wafers. For these simulations, we assume that the total hydrogen concentration (H_{tot}) is significantly lower than the background and emitter doping concentrations such that the effects of counter-doping remain negligible [67]. We note that although a change in the H_{tot} will have an impact on the absolute concentration of hydrogen within each charge state but will not affect the fractional probability of hydrogen occupying a particular state (which is what we are interested in). For simplicity within the model, we also assume that the initial concentration of hydrogen is distributed equally throughout the full thickness of the wafer, although it is well understood that hydrogen solubility, interactions with dopant atoms and diffusivity during firing should lead to an increased concentration amassing near the surface [64,68]. For these simulations, we consider an appropriate injection level under illumination to be $\Delta n = 1 \times 10^{15}$ cm^{-3}, as a midpoint to the Δn extracted before degradation (approximately Δn = 3–3.2 $\times$ 10^{15} cm^{-3} between 0.9 and 1 implied-suns) and after degradation (approximately $\Delta n = 7 \times 10^{14}$ cm^{-3} at 0.9 implied-suns). Although the injection level generally reduces during degradation, a carrier density of $\Delta n = 7 \times 10^{14}$ cm^{-3} is still four orders of magnitude greater than what is expected from thermally generated carriers in the dark. This reduction in Δn does not significantly influence the instantaneous distribution of hydrogen charge states and should not impact our model.

Fig. 7 shows the modelled fraction of charged hydrogen species as a function of depth into the silicon wafer. It is well established that H^- is the majority charge state of hydrogen within the *n-type* bulk, whereas H^+ is the dominant fraction within the diffused *p-type* region [65]. At a p-n junction, the Fermi level is pinned at the middle of the bandgap and given the asymmetry in the positions of the hydrogen donor (+/0) and acceptor (-/0) levels, H^+ is always the majority charge state [65,69]. Due to this asymmetry, the cross-over or transition between H^- and H^+ occurs on the *n-type* side of the metallurgical junction. If we take into consideration the coulombic attraction between the negatively charged

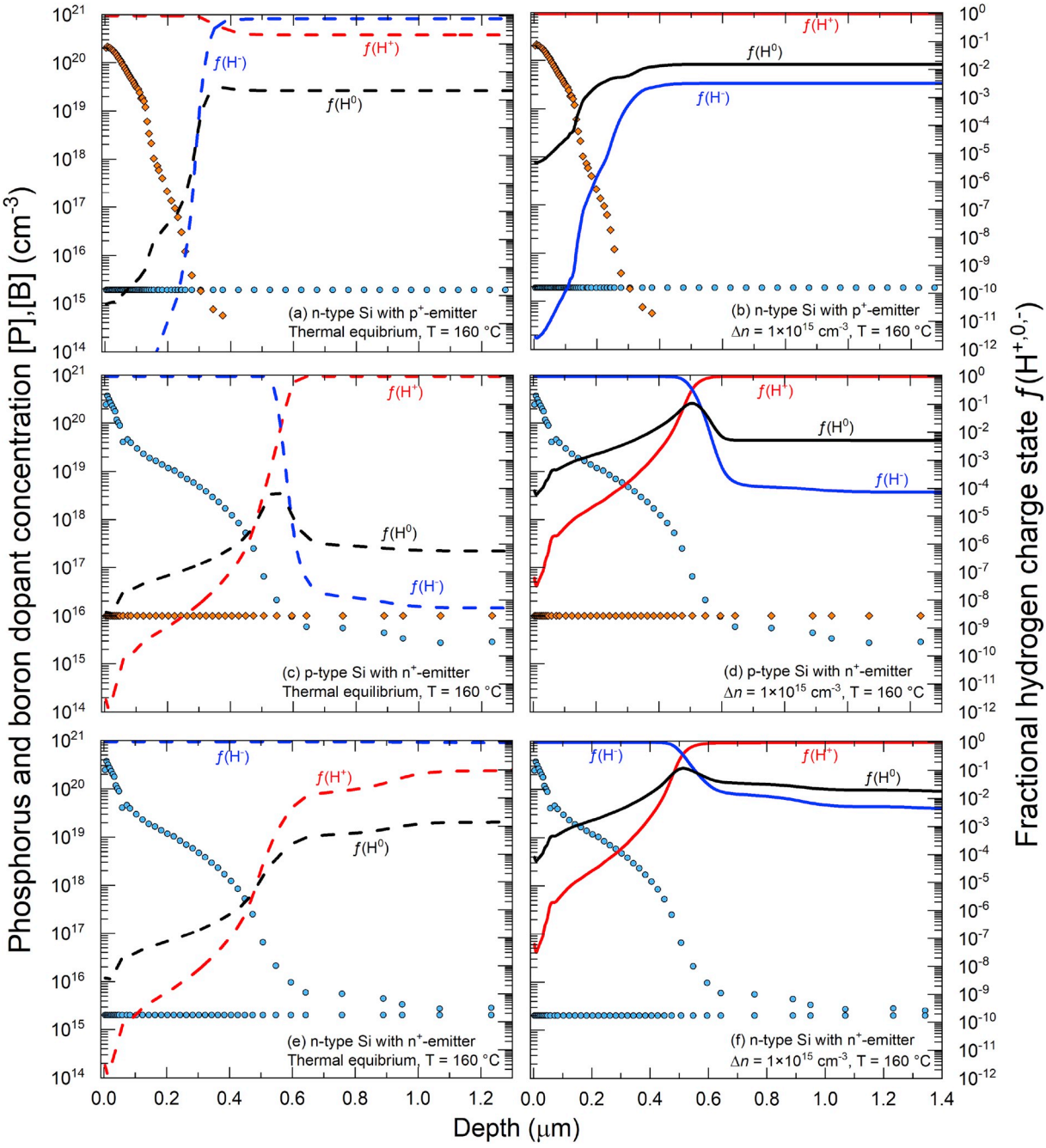

Fig. 7. The fraction of H^+ (red), H^0 (black) and H^- (blue) of the total monatomic hydrogen concentration as a function of depth under (a),(c),(e) thermal equilibrium at 160 °C and (b)(d)(f) with an added excess carrier injection of $\Delta n = 1 \times 10^{15}$ cm^{-3}. The measured ECV and background dopant phosphorus (blue circles) and boron (orange diamonds) profiles are displayed for (a),(b) *n-type* silicon with a boron-diffused emitter, (c),(d) *p-type* silicon with a phosphorus-diffused emitter and (e),(f) *n-type* silicon with a phosphorus diffused emitter. Note the dual axis where dopant concentrations and fractional hydrogen charge state are displayed on the left and right sides, respectively. (For interpretation of the references to color in this figure legend, the reader is referred to the Web version of this article.)

substitutional boron acceptor (B^-) and the H^+ hydrogen species as well as the similar attraction between the positively charged substitutional phosphorus donors (P^+) and the negative H^- species, we may be able to speculate on the motion of the charged species in the vicinity of the diffused layers.

The first observation is that in a boron-diffused *n-type* wafer, under thermal equilibrium (Fig. 7(a)), the majority charge state (H^-) within the bulk would be repelled away from negatively charged substitutional B^- cores in the emitter. With the addition of illumination and the generation of minority carriers, the shifting of the quasi-Fermi level towards mid-gap increases the occupation of holes at the energy level of interstitial hydrogen (Fig. 7(b)). This results in a near two orders of magnitude decrease in the fractional probability of hydrogen residing in the H^- state but an increase in the positive H^+ fraction by almost one order of magnitude. If our hypothesis that the migration of hydrogen across the junction is affected by coulombic attraction and repulsion is correct, this increase in H^+ would allow for an increased rate of migration into the emitter, thus resulting in the accelerated LeTID kinetics. Similarly, in a *p-type* substrate with a phosphorus-diffused emitter (Fig. 7(c) and (d)), an increase in over five orders of magnitude of the minority hydrogen species, H^-, under illumination, may also result in an accelerated migration of such species towards the positively

charged substitutional phosphorus cores (P^+) within the emitter. The most intriguing observation, however, is depicted in the modelling of a phosphorus-diffused *n-type* substrate, where the near-surface regions consists of a high-low junction instead of a p-n junction (Fig. 7(e) and (f)). Under thermal equilibrium, the primarily electron dominated diffused layer and bulk promotes a high occupancy of H^- throughout the entire substrate. These conditions would then allow the hydrogen to migrate rapidly into the heavily diffused region, possibly though coulombic forces and without any transition of charge states. This would be consistent with the rapid LeTID degradation and regeneration kinetics observed for this structure during dark annealing. Conversely, under illumination, where the Δn approaches the background phosphorus concentration, a transition of the quasi-Fermi level again raises the concentration of H^+ through an increased generation of holes, albeit this does not occur in the emitter where the doping concentration is significantly greater than the concentration of minority carriers. There is again, a scenario where a transition in charge state is required for the hydrogen to migrate into the emitter in addition to a repulsive force applied to the majority H^+ species. It would, therefore, be hypothesised that the resulting LeTID degradation or regeneration reaction kinetics would be reduced under such circumstances, thus consistent with the results observed in Section 3.1.

One point of contention may be raised from the results in Fig. 5 where the extracted rates for degradation and recovery for phosphorus-diffused n-type silicon wafers do not appear to differ under conditions of dark annealing and illuminated annealing, thus contradicting the theory postulated above. The illuminated annealing, however, was carried out at 0.02 kW/m^2 which we correlate to a Δn ceiling of approximately 1×10^{12} cm^{-3} in those particular samples. At these conditions, a transition to a majority H^+ in the *n-type* silicon bulk is not observed, unlike what is observed when the Δn is higher. This may provide an explanation as to why a reduction in the reaction rates is not observed. It is important, perhaps, in future work to investigate a range of higher illumination intensities >0.02 kW/m^2 and temperatures to understand the kinetics of degradation and recovery within these transition regimes.Using the interpretations of the model above, a predictive guess of the behavior of LeTID in an asymmetrically boron and phosphorus diffused *n-type* substrate can be made. At thermal equilibrium, we would expect to see a distribution of bulk hydrogen charge states similar to Fig. 7 (a) and (e) at the boron-diffused and phosphorus-diffused surfaces, respectively. Although any migration of the bulk H^- towards the boron-diffusion would be impeded, a rapid diffusion of H^- towards the high-low region on the opposing surface would occur. Under illumination, a switch in the dominant bulk hydrogen species to H^+ should now re-direct the migration of hydrogen towards the boron-emitter, thus also sporting a rapid LeTID degradation and regeneration reaction. To test this prediction, pre-fired *n-type* bifacial *Cz-Si* lifetime precursors consisting of an asymmetrical boron and phosphorus diffusion and dual-sided SiN_x:H passivation were acquired from *Jinko Solar*. LeTID testing was conducted *in-situ* at a temperature of 140 °C so that the minima may be observed clearly. The resulting evolution in lifetime during dark annealing and during light soaking with an illumination intensity of ≈1 kWm^{-2} is depicted in Fig. 8. The observed time required to reach maximum degradation under these conditions ($\approx 2.5 \times 10^3$ s) remains the same with additional carrier injection as predicted. This may suggest that, unlike a symmetrically diffused structures, a bifacial structure is expected to offer a pathway of rapid hydrogen movement across the diffused regions at all carrier densities.

4.3. Uncertainties in the involvement of hydrogen

The results above also raise several contradictions regarding the behaviour of hydrogen in silicon, some of which require further discussion. One may argue that the diffusivity of the various charge states of hydrogen differ significantly in silicon, often by orders of magnitude [60,70–72]. The reported diffusivity $D_{H(+/0/-)}$ of H^+ in *p-type* silicon at

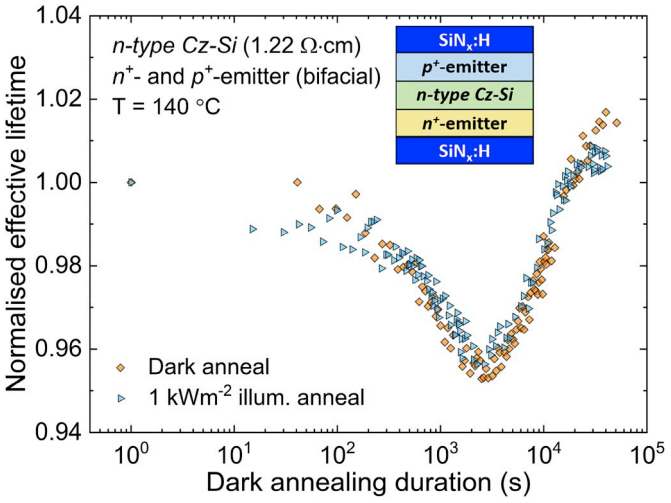

Fig. 8. Normalised effective lifetime, τ_{eff} (extracted at $\Delta n = 4 \times 10^{14}$ cm^{-3}) evolution of asymmetrically diffused *n-type Cz-Si* in the dark (diamonds) and under ≈1 kWm^{-2} illumination (triangles). The inset shows the structure of the sample used.

150 °C is $D_{H+} = 3 \times 10^{-13}$ cm^{2}s^{-1}, whereas H^- in *n-type* silicon is reported to have a diffusivity $D_{H-} = 3 \times 10^{-10}$ cm^{2}s^{-1}, that is, three orders of magnitude quicker [60]. In both *n-* and *p-type* silicon, the neutral charge state of hydrogen, H^0, is expected to have the greatest diffusivity ($D_{H0} = 1.8 \times 10^{-8}$ cm^{2}s^{-1}), due to its limited interaction with dopants and impurities [71]. If we consider our previous hypothesis in Ref. [39] that the recovery of LeTID may be related to the out-diffusion of hydrogen towards the wafer surfaces, it may be expected that in materials of opposing polarity or differing excess carrier injection, the variations in hydrogen charge state occupation should significantly alter the LeTID recovery reaction kinetics. The changes in recovery would subsequently reduce the perceived degradation time scale and extent. However, this would contradict both our results in Ref. [39], which demonstrated identical degradation time scales for *n-* and *p-type* silicon as well as the results in Figs. 3 and Fig. 8 also showing identical reaction kinetics and maximum degradation time scales. The alternative theory proposed by Bredemeier et al. in Ref. [46] postulated that hydrogen diffusing in from the surfaces were to passivate a defect responsible for LeTID, which would then be responsible for the subsequent recovery. Although this would be valid for both *p-* and *n-type* materials under illumination, where the dominant bulk hydrogen would be in the positive H^+ state, it again cannot explain the results in Fig. 8 where an *n-type* substrate annealed in the dark would also exhibit identical behaviours. Furthermore, differences in material purity (i.e., between *mc-Si* and *Cz-Si*) should also influence H diffusivity, particularly at the lower temperatures used to induce LeTID, largely due to the motion of hydrogen in silicon being trap-limited [73,74].

If the diffusivity of hydrogen is assumed not to influence LeTID behaviour, the other point to consider would be the absolute fractional hydrogen charge states present in our modelled structures. If we again examine the boron-diffused *n-type* structure and phosphorus diffused *p-type* structure at thermal equilibrium (Fig. 7 (a) and (c), respectively), there does not appear to be any point where the fractional concentration of a specific hydrogen charge state is equivalent in both structures, such that the average hydrogen diffusivity would be comparable. As mentioned previously, our simulations currently employ the assumption of a fixed interstitial hydrogen concentration profile throughout the bulk of the wafer. It is well known that the distribution of hydrogen after fast firing will often vary between materials. For example, there is consistent evidence that the solubility of hydrogen in *n-type* silicon is significantly lower than its *p-type* counterpart resulting in a large accumulation within the near-surface regions up to a depth of 2 μm [59,60]. This

interstitial hydrogen is also well known to act as a dopant, with its ability to passivate or neutralize both dopant atoms within diffused emitter layers as well as background dopants [75,76]. The reduction in effective doping as the hydrogen concentration approaches the local doping level will have a significant effect on the resulting charge state occupancy [67] as the quasi-Fermi level becomes driven toward mid-gap. To fully understand the impact of charge states on the kinetics of LeTID, further modelling using measured hydrogen profiles should be conducted.

4.4. LeTID and surface-related degradation

The final observation to address in this work is the rapid onset of SRD with the addition of illumination in phosphorus-diffused *n-type* samples. After the recovery of the bulk lifetime related to LeTID, a deterioration in the surface-related lifetime has been extensively reported and studied on *p-type* materials [42,61,77–79] and recently on *n-type* materials [39,44]. Both our previous work [39] and the work of Sperber et al. have attributed this SRD to a possible formation of hydrogen-induced extended defects as a result of an accumulation of hydrogen near the surface after long durations of light soaking and/or annealing. Both authors observed a faster and more pronounced degradation in *n-type* silicon substrates when compared to *p-type* silicon.

It is possible to explain why phosphorous diffused *n-type* substrates should experience a more rapid near-surface degradation, and how this is affected by illumination, within a model based on the redistribution of hydrogen from the wafer bulk to the surfaces. Such model may help to explain why the thermal activation energy associated with SRD in *n-type* Si (Section 3.2) may be lower than what has been reported for *p-type mc-Si* [21]. In order to do so, it is first important to consider how doping and surface charge affect the local carrier concentrations, and hence the fractions of interstitial hydrogen in each charge state as shown in Fig. 7. These fractions are crucial for the formation of recombination active defects. The second critical factor is the availability of interstitial hydrogen in the emitter/near surface region. Transport of hydrogen from the bulk is strongly affected by internal electric fields [64,80–82], while the local interstitial hydrogen concentration will also be affected by the trapping of hydrogen at dopant atoms within the emitter [83,84], which competes with other impurities and defects in the silicon to form complexes with hydrogen.

There is a significant body of work on the formation of recombination active defects by hydrogen, in the form of platelets and microcracks, at low temperatures [85–87]. This was first reported by Johnson et al. in 1987 [85], who observed planar micro-defects in *n-type* silicon samples exposed to hydrogen from a remote plasma. In contrast, the number of defects observed in *p-type* samples exposed to the same plasma showed were two orders of magnitude fewer. This was further investigated by Nickel et al. [86] who observed that a Fermi level within 0.26 eV below the conduction band was required for significant micro-defect formation and that the rate of formation increased rapidly as the Fermi level continued to approach the conduction band edge. The authors interpreted these results as evidence that the formation of hydrogen-induced extended defects requires a large fraction of both H^+ and H^- to be present. While it is unlikely that there is sufficient hydrogen available to form large platelets at the surface of our samples, it is likely that smaller extended defects and/or precursors may be the culprit for SRD. A large proportion of any phosphorous diffused emitter, and any (*p-* or *n-type*) surface passivated with a silicon nitride layer will have a Fermi level within 0.26 eV of the conduction band edge, and hence will be vulnerable to the formation of such defects. The second factor required for defect formation is then the availability of sufficient interstitial hydrogen.

As discussed in Section 4.2, the electric field due to a phosphorous emitter is such that it will always repel H^+ back towards the silicon bulk and sweep H^- towards the surface. While this accelerates hydrogen redistribution for *n-type* substrates with very low levels of illumination where H^- is dominant in the bulk, under most conditions, H^+ will be the dominant form in the silicon bulk and the electric field will act as a barrier for hydrogen migration. Fig. 8 shows how illumination reduces this barrier for both *p-* and *n-type* substrates and allows a greater flux of hydrogen into the emitter region, in a similar manner to previous reports using an applied bias to attempt to control the transport of hydrogen [80]. The simulations in Fig. 9 also show the apparent H^-/H^+ transition depth for *p-* and *n-type* silicon wafers with a phosphorus diffusion both at thermal equilibrium and with a carrier density of $\Delta n = 5 \times 10^{15}$ cm^{-3}, to the right of which is populated by the H^+ majority.

Illumination will also increase the concentration of holes in the emitter region as seen in Fig. 7. In order to understand the importance of the hole concentration, it is worth considering the deuterium SIMS profiles obtained by Pearton [88] on *n-* and *p-type* substrates of differing resistivities. When *n-type* substrates with resistivities of 1 Ω cm and below, in which H^- should be dominant, were exposed to a deuterium plasma at 125 °C, there was a distinct "shoulder" visible in the profiles that was much less pronounced in other samples. The authors attributed this to the formation of platelets in the near surface region. These profiles also show no evidence of dopant-hydrogen pairing, as seen in *p-type* samples under similar conditions. It was only when a diffusion was used to introduce P concentrations in excess of 10^{17} atoms/cm^3 that the formation of H–P pairs became significant. Even so, it was clear that the dissociation rate of these complexes is much greater than for H–B pairs as the concentration of H–P pairs was significantly below that of active P^+ ions. In addition, the "shoulder" caused by platelet formation was still very visible.

Based on these results we conclude that the most important effect of holes in the emitter is not an increase in the H^+ concentration. If the concentration of H^+ was really critical to formation of these defects we would expect their formation to be more pronounced in 1 Ω cm *n-type* than in 0.1 Ω cm and diffused samples, while the opposite appears to be true. Precursor formation might then be considered to be more likely via:

$$H^- + H^0 \rightarrow H_2^-$$

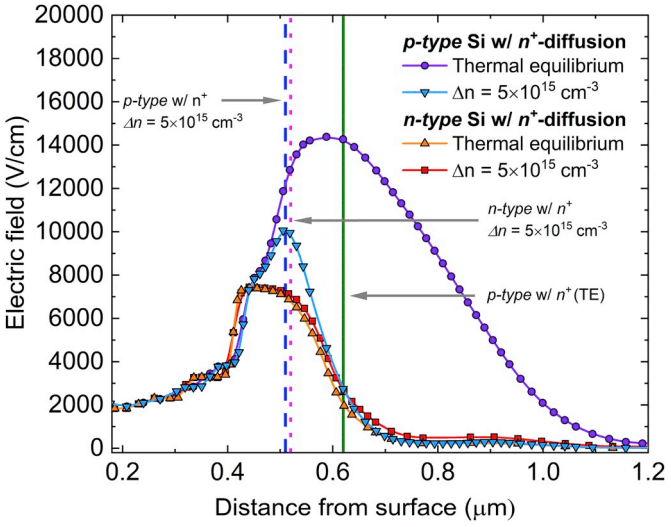

Fig. 9. Generated electric field as a function of depth for *n-* and *p-type* silicon substrates consisting of an n^+-diffusion, under conditions of thermal equilibrium or at a carrier density of $\Delta n = 5 \times 10^{15}$ cm^{-3}. Vertical lines mark the H^-/H^+ transition for *p-type* silicon at thermal equilibrium (green solid), *p-type* silicon at $\Delta n = 5 \times 10^{15}$ cm^{-3} (blue dashed) and *n-type* silicon at $\Delta n = 5 \times 10^{15}$ cm^{-3} (magenta dotted). Profiles are generated using the background and diffusion dopant profiles depicted in Fig. 2. (For interpretation of the references to color in this figure legend, the reader is referred to the Web version of this article.)

Rather than the initially more obvious:

$$H^- + H^+ \rightarrow H_2$$

H^0 at the tetrahedral site (H_T^0), which is also the lowest energy location for H^- ions, is reported to be an extremely rapid diffuser, with an activation energy of approximately 0.1 eV [89–91]. A precursor formation mechanism based on the generation of H_T^0 from H_T^- via hole capture or electron emission, followed by rapid diffusion of H_T^0 to the location of another H_T^0 (or potentially H_T^0), is thus at least plausible.

This leaves us with two potential roles that the hole concentration in the emitter might play. The first is to increase the generation rate of H_T^0, and the second is to increase the concentration of total interstitial hydrogen available by increasing the rate of dissociation of H–P pairs [92]. Both effects would serve to increase the rate of precursor/defect formation, in line with the experimental results in this work.

5. Conclusion

In this work, we have demonstrated an extended understanding of the mechanisms behind the formation of both LeTID and subsequent SRD in both *n*- and *p-type* silicon materials. By comparing *p*- and *n-type* substrates, we highlight the influence of the emitter polarity in modulating the LeTID defect formation and recovery kinetics. In the first section, we identify similarities in LeTID-related degradation behaviour present on vastly different materials, where *n*- and *p-type* silicon wafers occupy identical degradation time scales under illumination. By modelling the hydrogen charge state occupancy in the vicinity of a diffusion, we postulate that hydrogen is accelerated towards a high-low junction and repelled from a p-n junction. This understanding may allow future LeTID mitigation techniques to treat both materials simultaneously. In light of recent studies showing the detrimental effects of SRD subsequent to LeTID recovery, we show a correlation between illumination and temperature on this accelerated SRD phenomena in phosphorus-diffused *n-type Si* and report an extracted thermal activation energy of this SRD of 0.38 ± 0.10 eV. By evaluating the differences in electric fields brought about by phosphorus and boron diffusions, we conclude that the influence of such fields on hydrogen flux towards the surface can be used to explain an increase in SRD defect formation. In future work, the impact of pre-annealing processes on LeTID and SRD kinetics, in addition to the susceptibility of samples with various emitter profiles to such forms of degradation, will be investigated.

Author contribution

Daniel Chen: Conceptualization, Methodology, Writing – Original Draft, Investigation, Formal Analysis. **Phillip Hamer:** Formal Analysis, Writing – Original Draft. **Moonyong Kim:** Methodology, Formal Analysis, Writing – Original Draft. **Catherine Chan:** Conceptualization, Writing – Review and Editing, Supervision. **Alison Ciesla nee Wenham:** Writing – Review and Editing, Supervision, **Fiacre Rougieux**: Investigation, formation analysis. **Yuchao Zhang:** Investigation, Formal Analysis. **Malcolm Abbott:** Methodology, Writing – Review and Editing, Supervision. **Brett Hallam:** Conceptualization, Writing – Review and Editing, Supervision, Project administration, Funding acquisition.

Declaration of competing interest

The authors declare that they have no known competing financial interests or personal relationships that could have appeared to influence the work reported in this paper.

Acknowledgements

The authors would like to dedicate this work to the late Professor Stuart Wenham (15th July 195723rd December 2017) for his achievements and contributions to photovoltaics around the world. This work has been supported by the Australian Government through the Australian Renewable Energy Agency (ARENA) (ARENA 1-A060, 2017/RND010 and 2017/RND003) and the Australian Centre for Advanced Photovoltaics (ACAP, 1-SRI001), and the Australian Research Council (DE170100620). The views expressed herein are not necessarily the views of the Australian Government, and the Australian Government does not accept responsibility for any information or advice contained herein. Daniel Chen would like to acknowledge the support and contribution of the Australian Commonwealth Government through the Australian Government Research Training Program Scholarship. The authors would also like to acknowledge the SIRF processing team and Jinko Solar for assistance in sample preparation and Anastasia Soeriyadi, Shaoyang Liu, Chandany Sen, Utkarshaa Varshney, Aref Samadi, Carlos Vargas, Ziv Hameiri, Matthew Wright and Brendan Wright for useful discussions, experimental processing and characterisation. The authors would also like to thank the commercial partners of the ARENA 1-A060 advanced hydrogenation project, and the UK Institution of Engineering and Technology (IET) for their funding support for this work through the A.F. Harvey Engineering Prize.

Appendix A. Supplementary data

Supplementary data to this article can be found online at https://doi.org/10.1016/j.solmat.2019.110353.

References

[1] K. Ramspeck, S. Zimmermann, H. Nagel, A. Metz, Y. Gassenbauer, B. Brikmann, A. Seidl, Light induced degradation of Rear Passivated mc- Si solar cells, in: Proc. 27th Eur. Photovolt. Sol. Energy Conf., 2012, pp. 861–865, https://doi.org/10.4229/27THEUPVSEC2012-2DO.3.4.

[2] F. Kersten, P. Engelhart, H.-C. Ploigt, A. Stekolnikov, T. Lindner, F. Stenzel, M. Bartzsch, A. Szpeth, K. Petter, J. Heitmann, J.W. Müller, Degradation of multicrystalline silicon solar cells and modules after illumination at elevated temperature, Sol. Energy Mater. Sol. Cells 142 (2015) 83–86, https://doi.org/10.1016/j.solmat.2015.06.015.

[3] K. Petter, K. Hubener, F. Kersten, M. Bartzsch, F. Fertig, B. Kloter, J. Muller, Dependence of LeTID on brick height for different wafer suppliers with several resistivities and dopants, in: 9th Int. Work. Cryst. Silicon Sol. Cells., 2016.

[4] W. Kwapil, T. Niewelt, M.C. Schubert, Kinetics of carrier-induced degradation at elevated temperature in multicrystalline silicon solar cells, Sol. Energy Mater. Sol. Cells 173 (2017) 80–84, https://doi.org/10.1016/j.solmat.2017.05.066.

[5] C. Chan, T.H. Fung, M. Abbott, D. Payne, A. Wenham, B. Hallam, R. Chen, S. Wenham, Modulation of carrier-induced defect kinetics in multi-crystalline silicon PERC cells through dark annealing, Sol. RRL. 1 (2017) 1600028, https://doi.org/10.1002/solr.201600028.

[6] S. Liu, D. Payne, C. Vargas Castrillon, D. Chen, M. Kim, C. Sen, U. Varshney, Z. Hameiri, C. Chan, M. Abbott, S. Wenham, Impact of dark annealing on the kinetics of light- and elevated-temperature-induced degradation, IEEE J. Photovolt. 8 (2018) 1494–1502, https://doi.org/10.1109/JPHOTOV.2018.2866325.

[7] T. Luka, S. Großer, C. Hagendorf, K. Ramspeck, M. Turek, Intra-grain versus grain boundary degradation due to illumination and annealing behavior of multi-crystalline solar cells, Sol. Energy Mater. Sol. Cells 158 (2016) 43–49, https://doi.org/10.1016/j.solmat.2016.05.061.

[8] D.N.R. Payne, C.E. Chan, B.J. Hallam, B. Hoex, M.D. Abbott, S.R. Wenham, D. M. Bagnall, Rapid passivation of carrier-induced defects in p-type multi-crystalline silicon, Sol. Energy Mater. Sol. Cells 158 (2016) 102–106, https://doi.org/10.1016/j.solmat.2016.05.022.

[9] T.H. Fung, M. Kim, D. Chen, C.E. Chan, B.J. Hallam, R. Chen, D.N.R. Payne, A. Ciesla, S.R. Wenham, M.D. Abbott, A four-state kinetic model for the carrier-induced degradation in multicrystalline silicon: introducing the reservoir state, Sol. Energy Mater. Sol. Cells 184 (2018) 48–56, https://doi.org/10.1016/j.solmat.2018.04.024.

[10] D. Bredemeier, D. Walter, S. Herlufsen, J. Schmidt, Lifetime degradation and regeneration in multicrystalline silicon under illumination at elevated temperature, AIP Adv. 6 (2016), https://doi.org/10.1063/1.4944839.

[11] S. Liu, C. Chan, D. Chen, M. Kim, C. Sen, U. Varshney, B. Hallam, M. Abbott, S. Wenham, D. Payne, Investigation of temperature and illumination dependencies of carrier-induced degradation in p-type multi-crystalline silicon, in: AIP Conf. Proc., 2018, p. 130014, https://doi.org/10.1063/1.5049333.

[12] D. Bredemeier, D. Walter, S. Herlufsen, J. Schmidt, Understanding the light-induced lifetime degradation and regeneration in multicrystalline silicon, Energy Procedia 92 (2016) 773–778, https://doi.org/10.1016/j.egypro.2016.07.060.

[13] C.E. Chan, D.N.R. Payne, B.J. Hallam, M.D. Abbott, T.H. Fung, A.M. Wenham, B. S. Tjahjono, S.R. Wenham, Rapid stabilization of high-performance

multicrystalline P-type silicon PERC cells, IEEE J. Photovolt. 6 (2016) 1473–1479, https://doi.org/10.1109/JPHOTOV.2016.2606704.
[14] K. Nakayashiki, J. Hofstetter, A.E. Morishige, T.T.A. Li, D.B. Needleman, M. A. Jensen, T. Buonassisi, Engineering solutions and root-cause analysis for light-induced degradation in p-type multicrystalline silicon PERC modules, IEEE J. Photovolt. 6 (2016) 860–868, https://doi.org/10.1109/JPHOTOV.2016.2556981.
[15] R. Eberle, W. Kwapil, F. Schindler, M.C. Schubert, S.W. Glunz, Impact of the firing temperature profile on light induced degradation of multicrystalline silicon, Phys. Status Solidi Rapid Res. Lett. 10 (2016) 861–865, https://doi.org/10.1002/pssr.201600272.
[16] B.J. Hallam, P.G. Hamer, S. Wang, L. Song, N. Nampalli, M.D. Abbott, C.E. Chan, D. Lu, A.M. Wenham, L. Mai, N. Borojevic, A. Li, D. Chen, M.Y. Kim, A. Azmi, S. Wenham, Advanced hydrogenation of dislocation clusters and boron-oxygen defects in silicon solar cells, in: Energy Procedia, 2015, https://doi.org/10.1016/j.egypro.2015.07.113.
[17] K. Bothe, J. Schmidt, Electronically activated boron-oxygen-related recombination centers in crystalline silicon, J. Appl. Phys. 99 (2006), https://doi.org/10.1063/1.2140584, 013701.
[18] F. Fertig, R. Lantzsch, A. Mohr, M. Schaper, M. Bartzsch, D. Wissen, F. Kersten, A. Mette, S. Peters, A. Eidner, J. Cieslak, K. Duncker, M. Junghänel, E. Jarzembowski, M. Kauert, B. Faulwetter-Quandt, D. Meißner, B. Reiche, S. Geißler, S. Hörnlein, C. Klenke, L. Niebergall, A. Schönmann, A. Weihrauch, F. Stenzel, A. Hofmann, T. Rudolph, A. Schwabedissen, M. Gundermann, M. Fischer, J.W. Müller, D.J.W. Jeong, Mass production of p-type Cz silicon solar cells approaching average stable conversion efficiencies of 22 %, in: Energy Procedia, 2017, pp. 338–345, https://doi.org/10.1016/j.egypro.2017.09.308.
[19] D. Chen, M. Kim, B.V. Stefani, B.J. Hallam, M.D. Abbott, C.E. Chan, R. Chen, D.N. R. Payne, N. Nampalli, A. Ciesla, T.H. Fung, K. Kim, S.R. Wenham, Evidence of an identical firing-activated carrier-induced defect in monocrystalline and multicrystalline silicon, Sol. Energy Mater. Sol. Cells 172 (2017) 293–300, https://doi.org/10.1016/j.solmat.2017.08.003.
[20] T. Niewelt, R. Post, F. Schindler, W. Kwapil, M.C. Schubert, Investigation of LeTID where we can control it – application of FZ silicon for defect studies, in: 15th Int. Conf. Conc. Photovolt. Syst., 2019, p. 140006, https://doi.org/10.1063/1.5123893.
[21] D. Sperber, A. Schwarz, A. Herguth, G. Hahn, Bulk and surface-related degradation in lifetime samples made of Czochralski silicon passivated by plasma-enhanced chemical vapor deposited layer stacks, Phys. Status Solidi Appl. Mater. Sci. 215 (2018) 1–7, https://doi.org/10.1002/pssa.201800741.
[22] C. Vargas, Y. Zhu, G. Coletti, C. Chan, D. Payne, M. Jensen, Z. Hameiri, Recombination parameters of lifetime-limiting carrier-induced defects in multicrystalline silicon for solar cells, Appl. Phys. Lett. (2017), https://doi.org/10.1063/1.4977906, 092106.
[23] A.E. Morishige, M.A. Jensen, D.B. Needleman, K. Nakayashiki, J. Hofstetter, T. A. Li, T. Buonassisi, Lifetime spectroscopy investigation of light-induced degradation in p -type multicrystalline silicon PERC, IEEE J. Photovolt. 6 (2016) 1466–1472, https://doi.org/10.1109/JPHOTOV.2016.2606699.
[24] H. Deniz, J. Bauer, O. Breitenstein, Nickel precipitation in light and elevated temperature degraded multicrystalline silicon solar cells, Sol. RRL. 2 (2018) 1800170, https://doi.org/10.1002/solr.201800170.
[25] M.A. Jensen, A.E. Morishige, S. Chakraborty, R. Sharma, H.S. Laine, B. Lai, V. Rose, A. Youssef, E.E. Looney, S. Wieghold, J.R. Poindexter, J. Correa-Baena, T. Felisca, H. Savin, J.B. Li, T. Buonassisi, Solubility and diffusivity: important metrics in the search for the root cause of light- and elevated temperature-induced degradation, IEEE J. Photovolt. (2018) 1–8, https://doi.org/10.1109/JPHOTOV.2018.2791411.
[26] M. Wagner, F. Wolny, M. Hentsche, A. Krause, L. Sylla, F. Kropfgans, M. Ernst, R. Zierer, P. Bönisch, P. Müller, N. Schmidt, V. Osinniy, H.P. Hartmann, R. Mehnert, H. Neuhaus, Correlation of the LeTID amplitude to the Aluminium bulk concentration and Oxygen precipitation in PERC solar cells, Sol. Energy Mater. Sol. Cells 187 (2018) 176–188, https://doi.org/10.1016/j.solmat.2018.06.009.
[27] A.C. nee Wenham, S. Wenham, R. Chen, C. Chan, D. Chen, B. Hallam, D. Payne, T. Fung, M. Kim, S. Liu, S. Wang, K. Kim, A. Samadi, C. Sen, C. Vargas, U. Varshney, B.V. Stefani, P. Hamer, G. Bourret-Sicotte, N. Nampalli, Z. Hameiri, C. Chong, M. Abbott, Hydrogen-induced degradation, in: 2018 IEEE 7th World Conf. Photovolt. Energy Convers. (A Jt. Conf. 45th IEEE PVSC, 28th PVSEC 34th EU PVSEC), IEEE, 2018, https://doi.org/10.1109/PVSC.2018.8548100, pp. 0001–0008.
[28] D. Bredemeier, D.C. Walter, J. Schmidt, Lifetime degradation in multicrystalline silicon under illumination at elevated temperature: indications for the involvement of hydrogen, in: AIP Conf. Proc., 2018, https://doi.org/10.1063/1.5049320.
[29] T.H. Fung, C.E. Chan, B.J. Hallam, D.N.R. Payne, M.D. Abbott, S.R. Wenham, Impact of annealing on the formation and mitigation of carrier-induced defects in multi-crystalline silicon, Energy Procedia 124 (2017) 726–733, https://doi.org/10.1016/j.egypro.2017.09.087.
[30] R. Eberle, W. Kwapil, F. Schindler, S.W. Glunz, M.C. Schubert, Firing temperature profile impact on light induced degradation in multicrystalline silicon, in: Energy Procedia, Elsevier B.V., 2017, pp. 712–717, https://doi.org/10.1016/j.egypro.2017.09.082.
[31] U. Varshney, M. Abbott, A. Ciesla, D. Chen, S. Liu, C. Sen, M. Kim, S. Wenham, B. Hoex, C. Chan, Evaluating the impact of SiN x thickness on lifetime degradation in silicon, IEEE J. Photovolt. 9 (2019) 601–607, https://doi.org/10.1109/JPHOTOV.2019.2896671.
[32] M.A. Jensen, A. Zuschlag, S. Wieghold, D. Skorka, A.E. Morishige, G. Hahn, T. Buonassisi, Evaluating root cause: the distinct roles of hydrogen and firing in activating light- and elevated temperature-induced degradation, J. Appl. Phys. 124 (2018), https://doi.org/10.1063/1.5041756, 085701.
[33] D. Bredemeier, D.C. Walter, R. Heller, J. Schmidt, Impact of hydrogen-rich silicon nitride material properties on light-induced lifetime degradation in multicrystalline silicon, Phys. Status Solidi Rapid Res. Lett. 13 (2019) 1900201, https://doi.org/10.1002/pssr.201900201.
[34] C. Vargas, K. Kim, G. Coletti, D. Payne, C. Chan, S. Wenham, Z. Hameiri, Influence of silicon nitride and its hydrogen content of carrier-induced degradation in multicrystalline silicon, in: Proceeding 33rd Eur. Photovolt. Sol. Energy Conf. Exhib. Amsterdam, 2017, p. 561.
[35] T. Niewelt, F. Schindler, W. Kwapil, R. Eberle, J. Schön, M.C. Schubert, Understanding the light-induced degradation at elevated temperatures: similarities between multicrystalline and floatzone p-type silicon, Prog. Photovolt. Res. Appl. (2017) 1–10, https://doi.org/10.1002/pip.2954.
[36] F. Kersten, J. Heitmann, J.W. Müller, Influence of Al2O3 and SiNx passivation layers on LeTID, Energy Procedia 92 (2016) 828–832, https://doi.org/10.1016/j.egypro.2016.07.079.
[37] H.C. Sio, H. Wang, Q. Wang, C. Sun, W. Chen, H. Jin, D. Macdonald, Light and elevated temperature induced degradation in p-type and n-type cast-grown multicrystalline and mono-like silicon, Sol. Energy Mater. Sol. Cells 182 (2018) 98–104, https://doi.org/10.1016/j.solmat.2018.03.002.
[38] C. Vargas, S. Nie, D. Chen, C. Chan, B. Hallam, G. Coletti, Z. Hameiri, Degradation and recovery of n -type multi-crystalline silicon under illuminated and dark annealing conditions at moderate temperatures, IEEE J. Photovolt. 9 (2019) 355–363, https://doi.org/10.1109/JPHOTOV.2018.2885711.
[39] D. Chen, P.G. Hamer, M. Kim, T.H. Fung, G. Bourret-Sicotte, S. Liu, C.E. Chan, A. Ciesla, R. Chen, M.D. Abbott, B.J. Hallam, S.R. Wenham, Hydrogen induced degradation: a possible mechanism for light- and elevated temperature- induced degradation in n-type silicon, Sol. Energy Mater. Sol. Cells 185 (2018) 174–182, https://doi.org/10.1016/j.solmat.2018.05.034.
[40] C. Renevier, E. Fourmond, M. Forster, S. Parola, M. Le Coz, E. Picard, Lifetime degradation on n-type wafers with boron-diffused and SiO2/SiN-passivated surface, Energy Procedia 55 (2014) 280–286, https://doi.org/10.1016/j.egypro.2014.08.082.
[41] T. Niewelt, M. Selinger, N.E. Grant, W. Kwapil, J.D. Murphy, M.C. Schubert, Light-induced activation and deactivation of bulk defects in boron-doped float-zone silicon, J. Appl. Phys. 121 (2017) 185702, https://doi.org/10.1063/1.4983024.
[42] D. Sperber, A. Herguth, Instability of dielectric surface passivation quality at elevated temperature and illumination, Energy Procedia 92 (2016) 211–217, https://doi.org/10.1016/j.egypro.2016.07.061.
[43] D. Sperber, A. Graf, D. Skorka, A. Herguth, G. Hahn, Degradation of Surface Passivation on Crystalline Silicon and its Impact on Light Induced Degradation Experiments, 2017, pp. 1–9, https://doi.org/10.1109/JPHOTOV.2017.2755072.
[44] D. Sperber, A. Schwarz, A. Herguth, G. Hahn, Enhanced stability of passivation quality on diffused silicon surfaces under light-induced degradation conditions, Sol. Energy Mater. Sol. Cells 188 (2018) 112–118, https://doi.org/10.1016/j.solmat.2018.08.019.
[45] C. Sun, F.E. Rougieux, D. Macdonald, A unified approach to modelling the charge state of monatomic hydrogen and other defects in crystalline silicon, J. Appl. Phys. 117 (2015), https://doi.org/10.1063/1.4906465, 045702.
[46] D. Bredemeier, D.C. Walter, J. Schmidt, Possible candidates for impurities in mc-Si wafers responsible for light-induced lifetime degradation and regeneration, Sol. RRL. 2 (2018) 1700159, https://doi.org/10.1002/solr.201700159.
[47] P.J. Cousins, J.E. Cotter, The influence of diffusion-induced dislocations on high efficiency silicon solar cells, IEEE Trans. Electron Devices 53 (2006) 457–464, https://doi.org/10.1109/TED.2005.863535.
[48] Z. Hameiri, N. Borojevic, L. Mai, N. Nandakumar, K. Kim, S. Winderbaum, Should the refractive index at 633 nm be used to characterize silicon nitride films ?, 2016, pp. 2900–2904.
[49] Z. Hameiri, N. Borojevic, L. Mai, N. Nandakumar, K. Kim, S. Winderbaum, Low-absorbing and thermally stable industrial silicon nitride films with very low surface recombination, IEEE J. Photovolt. 7 (2017) 996–1003, https://doi.org/10.1109/JPHOTOV.2017.2706424.
[50] R. Sinton, A. Cuevas, A quasi-steady-state open-circuit voltage method for solar cell characterization, 16th Eur. Photovolt. Sol. Energy Conf. (2000) 1–4, doi:citeulike-article-id:6901946.
[51] A. Herguth, On the meaning(fullness) of the intensity unit “suns” in light induced degradation experiments, Energy Procedia 124 (2017) 53–59, https://doi.org/10.1016/j.egypro.2017.09.339.
[52] H. Nagel, C. Berge, A.G. Aberle, H. Nagel, C. Berge, A.G. Aberle, Generalized analysis of quasi-steady-state and quasi-transient measurements of carrier lifetimes in semiconductors Generalized analysis of quasi-steady-state and quasi-transient measurements of carrier lifetimes in semiconductors, J. Appl. Phys. 86 (1999) 6218–6221, https://doi.org/10.1063/1.371633.
[53] A. Richter, F. Werner, A. Cuevas, J. Schmidt, S.W. Glunz, Improved parameterization of auger recombination in silicon, Energy Procedia 27 (2012) 88–94, https://doi.org/10.1016/j.egypro.2012.07.034.
[54] J.M. Dorkel, P. Leturcq, Carrier mobilities in silicon semi-empirically related to temperature, doping and injection level, Solid State Electron. 24 (1981) 821–825, https://doi.org/10.1016/0038-1101(81)90097-6.
[55] S.W. Glunz, S. Rein, W. Warta, J. Knobloch, W. Wettling, Degradation of carrier lifetime in Cz silicon solar cells, Sol. Energy Mater. Sol. Cells 65 (2001) 219–229, https://doi.org/10.1016/S0927-0248(00)00098-2.
[56] A. Kimmerle, P. Rothhardt, A. Wolf, R.A. Sinton, Increased reliability for J0-analysis by QSSPC, Energy Procedia 55 (2014) 101–106, https://doi.org/10.1016/j.egypro.2014.08.087.

[57] C. Vargas, G. Coletti, C. Chan, D. Payne, Z. Hameiri, On the impact of dark annealing and room temperature illumination on p-type multicrystalline silicon wafers, Sol. Energy Mater. Sol. Cells 189 (2019) 166–174, https://doi.org/10.1016/j.solmat.2018.09.018.
[58] C. Dubé, J.I. Hanoka, D.B. Sandstrom, Hydrogen diffusion along passivated grain boundaries in silicon ribbon, Appl. Phys. Lett. 44 (1984) 425–427, https://doi.org/10.1063/1.94797.
[59] R. Rizk, P. De Mierry, D. Ballutaud, M. Aucouturier, D. Mathiot, Hydrogen diffusion in N-type Silicon.Comparison with P-type silicon, MRS Proc. 209 (1990) 573, https://doi.org/10.1557/PROC-209-573.
[60] D. Mathiot, Modeling of hydrogen diffusion in n-and p-type silicon, Phys. Rev. B. 40 (1989) 5867–5870. http://prb.aps.org/abstract/PRB/v40/i8/p5867_1.
[61] A. Herguth, C. Derricks, D. Sperber, A detailed study on light-induced degradation of Cz-Si PERC-type solar Cells : evidence of rear surface-related degradation, IEEE J. Photovolt. (2018) 1–12, https://doi.org/10.1109/JPHOTOV.2018.2850521.
[62] D. Sperber, A. Graf, D. Skorka, A. Herguth, G. Hahn, Degradation of surface passivation and its impact on light-induced degradation experiments, IEEE J. Photovolt. 7 (2017) 1627–1634, https://doi.org/10.1109/JPHOTOV.2017.2755072.
[63] T. Luka, S. Großer, C. Hagendorf, K. Ramspeck, M. Turek, Intra-grain versus grain boundary degradation due to illumination and annealing behavior of multi-crystalline solar cells, Sol. Energy Mater. Sol. Cells 158 (2016) 43–49, https://doi.org/10.1016/j.solmat.2016.05.061.
[64] P. Hamer, B. Hallam, R.S. Bonilla, P.P. Altermatt, P. Wilshaw, S. Wenham, Modelling of hydrogen transport in silicon solar cell structures under equilibrium conditions, J. Appl. Phys. 123 (2018), https://doi.org/10.1063/1.5016854, 043108.
[65] C. Herring, N.M. Johnson, C.G. Van de Walle, Energy levels of isolated interstitial hydrogen in silicon, Phys. Rev. B. 64 (2001) 125209, https://doi.org/10.1103/PhysRevB.64.125209.
[66] B.J. Hallam, P.G. Hamer, S.R. Wenham, M.D. Abbott, A. Sugianto, A.M. Wenham, C.E. Chan, G. Xu, J. Kraiem, J. Degoulange, R. Einhaus, Advanced bulk defect passivation for silicon solar cells, IEEE J. Photovolt. 4 (2014) 88–95, https://doi.org/10.1109/JPHOTOV.2013.2281732.
[67] R. Chen, A.M. Ciesla, D. Chen, C.E. Chan, P.G. Hamer, B.J. Hallam, S.R. Wenham, Impact of the impurity concentration on modulating charge state occupation in silicon, in: 2018 IEEE 7th World Conf. Photovolt. Energy Convers. (A Jt. Conf. 45th IEEE PVSC, 28th PVSEC 34th EU PVSEC), IEEE, 2018, https://doi.org/10.1109/PVSC.2018.8548195, pp. 0053–0057.
[68] B.L. Sopori, X. Deng, J.P. Benner, A. Rohatgi, P. Sana, S.K. Estreicher, Y.K. Park, M. A. Roberson, Hydrogen in silicon: a discussion of diffusion and passivation mechanisms, Sol. Energy Mater. Sol. Cells 41–42 (1996) 159–169, https://doi.org/10.1016/0927-0248(95)00098-4.
[69] J. Zhu, N.M. Johnson, C. Herring, State of Hydrogen in Silicon, 1990, p. 41.
[70] L. Bilteanu, M. Posselt, J.-P. Crocombette, Hydrogen diffusion in silicon - an ab initio study of hydrogen kinetic properties in silicon, ArXiv.Org, Condens. Matter Mater. Sci. (2011) 6455. arXiv:1111, http://arxiv.org/abs/1111.6455.
[71] A. Van Wieringen, N. Warmoltz, On the permeation of hydrogen and helium in single crystal silicon and germanium at elevated temperatures, Physica 22 (1956) 849–865, https://doi.org/10.1016/S0031-8914(56)90039-8.
[72] B.J. Hallam, A.M. Ciesla, C.C. Chan, A. Soeriyadi, S. Liu, A.M. Soufiani, M. Wright, S. Wenham, Overcoming the challenges of hydrogenation in silicon solar cells, Aust. J. Chem. 71 (2018) 743, https://doi.org/10.1071/ch18271.
[73] T. Zundel, J. Weber, Trap-limited hydrogen diffusion in boron-doped silicon, Phys. Rev. B. 46 (1992) 2071–2077.
[74] C.P. Herrero, M. Stutzmann, A. Breitschwerdt, P.V. Santos, Trap-limited hydrogen diffusion in doped silicon, Phys. Rev. B. 41 (1990) 1054–1058, https://doi.org/10.1103/PhysRevB.41.1054.
[75] C.T. Sah, J.Y.C. Sun, J.J.T. Tzou, Deactivation of the boron acceptor in silicon by hydrogen, Appl. Phys. Lett. 43 (1983) 204–206, https://doi.org/10.1063/1.94287.
[76] J.I. Pankove, R.O. Wance, J.E. Berkeyheiser, Neutralization of acceptors in silicon by atomic hydrogen, Appl. Phys. Lett. 45 (1984) 1100–1102, https://doi.org/10.1063/1.95030.
[77] K. Kim, R. Chen, D. Chen, P. Hamer, A. Ciesla Nee Wenham, S. Wenham, Z. Hameiri, Degradation of surface passivation and bulk in p-type monocrystalline silicon wafers at elevated temperature, IEEE J. Photovolt. 9 (2019) 97–105, https://doi.org/10.1109/JPHOTOV.2018.2878791.
[78] D. Sperber, F. Furtwängler, A. Herguth, G. Hahn, On the stability of dielectric passivation layers under illumination and temperature treatments, in: Proc. 32nd Eur. Photovolt. Sol. Energy Conf. Exhib., 2016, pp. 523–526, https://doi.org/10.4229/EUPVSEC20162016-2DO.3.4.
[79] D. Sperber, A. Heilemann, A. Herguth, G. Hahn, Temperature and light induced changes in bulk and passivation quality of boron-doped float-zone silicon coated with SiNx:H, IEEE J. Photovolt. (2017) 1–8, https://doi.org/10.1109/JPHOTOV.2017.2649601.
[80] P. Hamer, C. Chan, R.S. Bonilla, B. Hallam, G. Bourret-Sicotte, K.A. Collett, S. Wenham, P.R. Wilshaw, Hydrogen induced contact resistance in PERC solar cells, Sol. Energy Mater. Sol. Cells 184 (2018), https://doi.org/10.1016/j.solmat.2018.04.036.
[81] A.J. Tavendale, D. Alexiev, A.A. Williams, Field drift of the hydrogen-related, acceptor-neutralizing defect in diodes from hydrogenated silicon, Appl. Phys. Lett. 47 (1985) 316–318.
[82] N.M. Johnson, C. Herring, Diffusion of negatively charged hydrogen in silicon, Phys. Rev. B. 46 (1992) 15554.
[83] N.M. Johnson, C. Herring, D.J. Chadi, Interstitial hydrogen and neutralization of shallow-donor impurities in single-crystal silicon, Phys. Rev. Lett. 56 (1986) 769.
[84] C. Sah, J.Y. Sun, J.J. Tzou, Deactivation of the boron acceptor in silicon by hydrogen, Appl. Phys. Lett. 43 (1983) 204–206.
[85] N.M. Johnson, F.A. Ponce, R.A. Street, R.J. Nemanich, Defects in c-Si induced by hydrogenation, Phys. Rev. B. 35 (1987) 4166–4169.
[86] N.H. Nickel, G.B. Anderson, N.M. Johnson, J. Walker, Nucleation of hydrogen-induced platelets in silicon, Phys. Rev. B Condens. Matter Mater. Phys. 62 (2000) 8012–8015, https://doi.org/10.1103/PhysRevB.62.8012.
[87] E. V Lavrov, J. Weber, Evolution of hydrogen platelets in silicon determined by polarized Raman spectroscopy, Phys. Rev. Lett. 87 (2001) 185502.
[88] S.J. Pearton, Diffusion of hydrogen in n-type Si, Mater. Sci. Eng. B 23 (1994) 130–136.
[89] K. Bonde-Nielsen, B. Bech-Nielsen, J. Hansen, E. Andersen, J.U. Andersen, Bond-centered hydrogen in silicon studied by in situ deep-level transient spectroscopy, Phys. Rev. B Condens. Matter Mater. Phys. 60 (1999) 1716–1728, https://doi.org/10.1103/PhysRevB.60.1716.
[90] K.B. Nielsen, L. Dobaczewski, S. Søgård, B.B. Nielsen, Acceptor state of monoatomic hydrogen in silicon and the role of oxygen, Phys. Rev. B. 65 (2002) 75205, https://doi.org/10.1103/PhysRevB.65.075205.
[91] S.K. Estreicher, A. Docaj, M.B. Bebek, D.J. Backlund, M. Stavola, Hydrogen in C-rich Si and the diffusion of vacancy–H complexes, Phys. Status Solidi 209 (2012) 1872–1879.
[92] N.M. Johnson, C. Herring, Kinetics of minority-carrier-enhanced dissociation of hydrogen-dopant complexes in semiconductors, Phys. Rev. B. 45 (1992) 11379.